A Protein Profile of Visceral Adipose Tissues Linked to Early Pathogenesis of Type 2 Diabetes Mellitus*[S]

Su-Jin Kim‡§¶, Sehyun Chae¶‖, Hokeun Kim‡, Dong-Gi Mun‡, Seunghoon Back‡, Hye Yeon Choi, Kyong Soo Park‡‡, Daehee Hwang§‖§§, Sung Hee Choi**§§, and Sang-Won Lee‡§§**

Adipose tissue is increasingly recognized as an endocrine organ playing important pathophysiological roles in metabolic abnormalities, such as obesity, cardiovascular disease, and type 2 diabetes mellitus (T2DM). In particular, visceral adipose tissue (VAT), as opposed to subcutaneous adipose tissue, is closely linked to the pathogenesis of insulin resistance and T2DM. Despite the importance of VAT, its molecular signatures related to the pathogenesis of T2DM have not been systematically explored. Here, we present comprehensive proteomic analysis of VATs in drug-naïve early T2DM patients and subjects with normal glucose tolerance. A total of 4,707 proteins were identified in LC-MS/MS experiments. Among them, 444 increased in abundance in T2DM and 328 decreased. They are involved in T2DM-related processes including inflammatory responses, peroxisome proliferator-activated receptor signaling, oxidative phosphorylation, fatty acid oxidation, and glucose metabolism. Of these proteins, we selected 11 VAT proteins that can represent alteration in early T2DM patients. Among them, up-regulation of FABP4, C1QA, S100A8, and SORBS1 and down-regulation of ACADL and PLIN4 were confirmed in VAT samples of independent early T2DM patients using Western blot. In summary, our profiling provided a comprehensive basis for understanding the link of a protein profile of VAT to early pathogenesis of T2DM. ***Molecular & Cellular Proteomics 13: 10.1074/mcp.M113.035501, 811–822, 2014.***

Adipose tissue is a complex endocrine organ in which mature adipocytes coexist with connective tissue matrix, immune cells, the stromal vascular fraction of cells, and blood vessels (1, 2). The different fat depots, such as visceral adipose tissue (VAT)[1] and subcutaneous adipose tissue (SAT), release different types of adipokines and have distinct responses to hormones or mitochondrial density (3–5). In particular, VATs located in intra-abdominal cavities and around internal organs (1, 4, 6) release adipokines and free fatty acids (5, 7–9), thereby influencing the physiology of other organs (*e.g.* liver, pancreas, brain, or muscle). For example, the adipokines released from VATs regulate lipid metabolism in liver (10, 11). Thus, alterations in VATs lead to metabolic disorders with systemic inflammation, including atherosclerosis, obesity, dyslipidemia, cardiovascular disease, insulin resistance, type 2 diabetes mellitus (T2DM), and hypertension (7, 8, 12–15).

In patients with T2DM, the accumulation of visceral fat has been reported to have a high correlation with peripheral insulin resistance, especially hepatic insulin resistance (13, 16). Moreover, higher amounts of VATs are commonly observed in patients with metabolic diseases and other ectopic fat deposition (13, 17). The alteration in the metabolic milieu and adipokine secretion of VATs in patients with insulin resistance

From the ‡Department of Chemistry, Research Institute for Natural Sciences, Korea University, Seoul, 136-701, Republic of Korea; §Center for Systems Biology of Plant Senescence and Life History, Institute for Basic Science, DGIST, Daegu, 711-873, Republic of Korea; ‖School of Interdisciplinary Bioscience and Bioengineering, POSTECH, Pohang, Kyungbuk, 790-784, Republic of Korea; **Seoul National University Bundang Hospital, Internal Medicine, Endocrinology and Metabolism, Seoul National University College of Medicine, Gumidong 300, Bundang, Seongnam, Gyeonggi-do, 463-707, Republic of Korea; ‡‡Internal Medicine, Endocrinology and Metabolism, Seoul National University College of Medicine, Seoul 110-799, Republic of Korea

Received October 27, 2013, and in revised form, December 20, 2013

Published, MCP Papers in Press, January 8, 2014, DOI 10.1074/mcp.M113.035501

Author contributions: D.H., S. Choi, and S.L. designed research; S.K., S. Chae, H.C., K.P., D.H., S. Choi, and S.L. performed research; S.K., S. Chae, H.K., D.M., S.B., D.H., S. Choi, and S.L. analyzed data; S.K., S. Chae, D.H., S. Choi, and S.L. wrote the paper.

[1] The abbreviations used are: VAT, visceral adipose tissue; T2DM, type 2 diabetes mellitus; NGT, normal glucose tolerance; SAT, subcutaneous adipose tissue; SNUBH, Seoul National University Bundang Hospital; *i*PE-MMR, integrated post-experiment monoisotopic mass refinement; UMC, unique mass class; AMT DB, accurate mass and time tag database; NET, normalized elution time; FDR, false discovery rate; DEP, differentially expressed protein; GO, Gene Ontology; GOBP, Gene Ontology biological process; S100A, S100 calcium binding protein A; C1QA, complement component 1, q subcomponent, A chain; SORBS1, sorbin and SH3 domain containing 1; ACADL, acyl-CoA dehydrogenase, long chain; FABP4, fatty acid binding protein 4; PLIN, perilipin; ECM, extracellular matrix.

and T2DM relative to healthy controls has been considered as important pathophysiology for developing T2DM and cardiovascular disease (13, 15). Thus, these data suggest that VATs can serve as a key target organ from which novel molecules or pathways linked to the pathogenesis of T2DM, cardiovascular disease, or obesity can be identified.

The search for novel proteins or pathways linked to complex human diseases has been facilitated by the use of proteomic technologies. Several proteomic studies have provided global proteome profiles of tissue and serum samples from T2DM patients or mouse models and identified protein profiles associated with the pathogenesis of T2DM (18–22). For example, Li *et al.* (18) identified 68 proteins elevated in the sera of T2DM patients and found that the complement system is significantly associated with T2DM. Among the 68 proteins, they further validated ficolin-3, an upstream activator of the complement pathway, in independent samples. In the case of adipose cells or tissues, Adachi *et al.* (23) identified 3,287 proteins from mouse 3T3-L1 adipocytes, and Xie *et al.* (24) identified 1,493 proteins from abdominal SATs of three healthy individuals. These studies showed that these proteomes are involved in adipose functions that can thus serve as useful resources for various studies of adipose-related diseases. However, these proteomes were measured from adipose cells and SATs under nonpathogenic conditions. Comprehensive proteomes of VATs in T2DM patients and subjects with normal glucose tolerance (NGT), as well as comparative analysis of proteomes between subjects with T2DM and NGT, have not been systematically explored in terms of the molecular signatures related to the pathogenesis of T2DM.

Here, we have undertaken an extensive proteome profiling of VATs obtained from drug-naïve early T2DM patients (duration of diagnosis of diabetes within 5 years) and subjects with NGT. In this study, we analyzed whole VATs, including adipocytes and vessel and inflammatory cells, after carefully removing blood, to produce the data representing cross-talk among these cells during the development of T2DM-related alteration in VATs. A sample preparation method utilizing filter-aided sample preparation (25) that incorporated prior removal of the lipid layer was used to improve the extraction of proteins from VATs with high lipid contents. Furthermore, the use of ultra-high-pressure nano-LC-MS/MS coupled with extensive fractionation generated a comprehensive proteome of VATs, including 22,250 peptides of 4,707 proteins. From among them, we selected hundreds of differentially expressed proteins in VATs of T2DM patients that are involved in T2DM-related processes. Finally, of these proteins, we selected six proteins indicative of early pathogenesis of T2DM in VATs.

EXPERIMENTAL PROCEDURES

Patient Enrollment and Sample Collection—We collected two independent sets of whole VATs from T2DM and healthy subjects who underwent elective abdominal surgery in Seoul National University Bundang Hospital (SNUBH). The first set of five T2DM patients and six healthy subjects was used for the proteome profiling (supplemental Fig. S1). We enrolled T2DM patients who had been diagnosed with diabetes within the past 5 years based on American Diabetes Association criteria (26) and had undergone only lifestyle modification, without taking antidiabetic medication (drug naïve). They showed normal body mass index values ($<$25 kg/m^2) and had no past history of major adverse cardiovascular events, acute inflammatory diseases, or cancer. We excluded drug-naïve subjects with uncontrolled diabetes showing hemoglobin A1c $>$ 8%. The control group with NGT was enrolled based on the same American Diabetes Association criteria. They were also confirmed by means of a 75-g oral glucose tolerance test and were age and sex matched. To confirm the validity of the selected proteins by Western blotting, we assembled a second test set that comprised 10 T2DM patients and 10 individuals with NGT who had undergone elective cholecystectomy and thoracic surgery in SNUBH. Informed consent was obtained from all subjects. This study was conducted according to the Declaration of Helsinki and was approved by ethics committees of SNUBH (SNUBH IRB#B-1203/147–006, #A111218-CP02). The clinical characteristics of all enrolled patients for proteome profiling and for confirming candidate proteins are described in supplemental Table S1.

Homogenization and Protein Extraction—Fat samples from surgery were immediately sent to our laboratory, where they were washed three times in phosphate-buffered saline (PBS) solution to remove blood clots and stored in a −80 °C refrigerator. Surgeons intended to collect VATs from the same area when possible, and these samples were mostly omental fat from close to the transverse colon. Frozen VATs were slowly thawed in ice for the next step and then very carefully and gently washed in ice-cold PBS to remove excessive blood contamination. Fat tissues were minced with scissors into small pieces, collected in test tubes, transferred to FastPrep tubes containing mini beads, and homogenized in 0.1 M Tris-HCl (pH 7.6) by a FastPrep beater (Bio101Savant, Carlsbad, CA) until there were no tissue pieces. The lysate was transferred to a new tube and centrifuged at 14,000*g* for 15 min at 4 °C, and the rest (the floating mature adipocytes and the stromal vascular fraction cell pellet) except the lipid portion on the top was carefully recovered (27, 28). Removal of the lipid layer was very important, as it interferes with protein solubilization and the subsequent separation of proteins from lipid (29, 30). The lysate was transferred to a new tube, and the protein concentration was determined using a BCA protein assay (Pierce, Rockford, IL) and bovine serum albumin (Pierce) as a standard protein for the assay. No depletion of abundant proteins was attempted.

Enzymatic Digestion—Peptide samples were prepared via filter-aided sample preparation (25), with certain steps slightly modified to improve protein extraction. Briefly, 100 μg of protein lysate was reduced in 100 μl of SDT (4% SDS and 0.1 M DTT in 0.1 M Tris-HCl, pH 7.6) for 45 min at 37 °C and then boiled for 10 min to increase denaturation. After the protein lysate in 100 μl of SDT had been mixed with 200 μl of 8 M urea in a Microcon filter (YM-30, Millipore Corporation, Bedford, MA), the filter was centrifuged at 14,000*g* at 20 °C for 60 min. All centrifugation steps were performed at 20 °C. To remove residual SDS, 200 μl of 8 M urea in 0.1 M Tris-HCl (pH 8.5) was added to the filter before the filter was centrifuged at 14,000*g* ($\times$2). Subsequently, 100 μl of 50 mM iodoacetamide in 8 M urea in 0.1 M Tris-HCl was added to the concentrate for alkylation for 25 min at 25 °C in the dark, and this was followed by centrifugation at 14,000*g* for 30 min to remove the alkylation reagent. The resulting sample was rinsed again with 200 μl of 8 M urea in 0.1 M Tris-HCl. Finally, urea buffer was exchanged by adding and centrifuging 100 μl of 50 mM NH_4HCO_3 at 14,000*g* for 40 min ($\times$2). The protein sample was subjected to proteolytic digestion using trypsin (1:50 enzyme-to-protein ratio (w/w), Promega, Madison, WI) and 0.1% (w/v) RapiGest (Waters, Milford, MA) (28, 31) in 50 mM NH_4HCO_3 with initial mixing at 600 rpm in a thermomixer (Eppendorf, Hamburg, Germany) for 1 min at 37 °C and

overnight digestion without agitation. After the first digestion, a second trypsin digestion (1:100 enzyme-to-protein ratio) was carried out for 6 h. The digested peptides were eluted from the filter via centrifugation at 14,000*g* for 30 min, the filter was rinsed with 60 μl of 50 mM NH_4HCO_3 and centrifuged at 14,000*g* for 20 min, and the flow-through was mixed with the first eluent. The eluent was treated with 5 μl of formic acid, incubated for 45 min at 37 °C, and then centrifuged at 14,000*g* for 10 min to remove the RapiGest reagent. The supernatant was transferred to a new tube and dried completely using a SpeedVac concentrator (Thermo, San Jose, CA). Dried peptides were stored at −80 °C.

Isoelectric Focusing of Peptides—10 μg of each of 10 fat peptide samples (5 NGT and 5 T2DM) were collected and then pooled (total = 100 μg). The pooled sample was divided into 26 fractions using a 3100 OFFGEL Fractionator (Agilent Technologies, Santa Clara, CA) (32). Briefly, a 24-cm-long immobilized pH gradient gel strip (pH 3–10, GE Healthcare Life Sciences) was rehydrated for 15 min with the addition of 25 μl of rehydration solution to each well of a 24-well tray. The 100 μg of pooled peptides was dissolved in 0.72 ml of distilled water. The peptide solution was mixed with 2.88 ml of OFFGEL stock solution, and 150 μl of the total of 3.6 ml was load into each of 24 wells. The peptide sample was focused at 20 °C with a maximum current of 50 μA, and the voltage range was from 500 to 8,000 V until reaching 50 kVh. After the focusing, the peptides were recovered from the 24 wells. We also collected peptides from both the anode end (consisting of peptides having pI values less than 3) and the cathode end (consisting of peptides having pI values greater than 10). Thus, 26 fractions were prepared in total. Glycerol was removed by desalting in a spin column (Harvard Apparatus, Holliston, MA) before each of the fractionated peptides was vacuum-dried. Dried peptides were stored at −80 °C.

LC-MS/MS Experiments—A total of 59 LC-MS/MS datasets from normal, diabetes mellitus, and OFFGEL fractions of pooled samples were separated using a modified version of the nanoACQUITY UPLC (NanoA, Waters, Milford, MA) system (33). An analytical column (75 μm inner diameter × 360 μm outer diameter × 70 cm length) was manufactured in-house by acetonitrile slurry packing a fused-silica capillary (Polymicro Technologies, Phoenix, AZ) with C18 materials (3 μm diameter, 300 Å pore size; Jupiter, Phenomenex, Torrance, CA). The solid phase extraction column was prepared by packing the same C18 materials into the 1-cm-long liner (250 μm inner diameter) of an internal reducer (1/16 inch to 1/32 inch, VICI, Houston, TX). The column temperature was set at 50 °C using a semi-rigid gasline heater (1/4-inch inner diameter, 60-cm length, WATLOW, St. Louis, MO.) (34). For 26 OFFGEL fraction samples, the LC separation gradient was 98% solvent A (0.1% formic acid in H_2O) for 5 min, 2% to 50% solvent B (0.1% formic acid in 99.9% acetonitrile) in 115 min, 50% to 80% solvent B in 10 min, and 80% solvent B in 10 min. For the triplicate LC-MS/MS experiments on the unfractionated individual samples, the LC gradient was 98% solvent A (0.1% formic acid in H_2O) for 5 min, 2% to 50% solvent B (0.1% formic acid in 99.9% acetonitrile) in 235 min, 50% to 80% solvent B in 10 min, and 80% solvent B in 10 min. The flow rate of the mobile phase was set at 400 nl/min. A 7-tesla Fourier transform ion cyclotron resonance mass spectrometer (LTQ-FT, Thermo Electron, San Jose, CA) was used to collect the mass spectra. The eluted peptides from the LC were ionized at an electrospray potential of 2.0 kV. The electrospray ionization emitter was manufactured by chemical etching of a fused-silica capillary emitter (20 μm inner diameter × 150 μm outer diameter) (35). The temperature of the desolvation capillary was set at 250 °C. MS precursor ion scans (*m/z* 500–2,000) were acquired in a full-profile mode with an automatic gain control target value of 1×10^6, a mass resolution of 1×10^5, and a maximum ion accumulation time of 500 ms. The mass spectrometer was operated in data-dependent tandem MS mode; the seven most abundant ions detected in a precursor MS scan were dynamically selected for MS/MS experiments incorporating a dynamic exclusion option (exclusion mass width low, 1.10 Th; exclusion mass width high, 2.10 Th; exclusion list size, 120; exclusion duration, 30 s) to prevent reacquisition of MS/MS spectra of the same peptides. Collision-induced dissociations of the precursor ions were performed in an ion trap (LTQ) with the collisional energy and isolation width set to 35% and 3 Th, respectively. The Xcalibur software package (v. 2.0 SR2, Thermo Electron) was used to construct the experimental methods.

Database Search for Peptide Identification—The integrated post-experiment monoisotopic mass refinement (*i*PE-MMR) method was used to process the LC-MS/MS data and was previously demonstrated to accurately assign precursor masses to tandem mass spectrometric data before a subsequent protein database search (36). Briefly, DeconMSn (37) was used to generate MS/MS data (DTA files) whose precursor masses were further corrected and refined through PE-MMR (38). The resultant mass-refined DTA files were subjected to multivariate mass error correction using DtaRefinery (39, 40). The resultant MS/MS data after *i*PE-MMR processes were searched against a composite target-decoy database that contains human data (IPI v. 3.86, 91,550 entries) and its reversed complements using the SORCERER™-SEQUEST (v. 3.5) search algorithm (Sage-N Research, Milpitas, CA). The searches were performed allowing for semi-tryptic peptides, and the maximum allowable number of missed cleavages was 3. The mass tolerance was 10 ppm for precursor ions and 1 Da for fragment ions. The carbamidomethylation of cysteine (57.021460 Da) was used as a static modification. Variable modification options were used for the oxidation of methionine (15.994920 Da) and the carbamylation of N-terminal sites (43.005810 Da). The search results were filtered using an estimated false discovery rate (FDR). The FDR of peptide assignments was estimated through a composite target-decoy database search. The values of Xcorr and the ΔCn threshold for the 1% FDR were used to obtain peptide I.D.s (41).

Assigning MS Intensity to Peptide Identification—An MS intensity-based label-free quantitation method was applied to adipose tissue LC-MS/MS data (33 LC-MS/MS data) as described previously (41). Briefly, during PE-MMR analysis, MS features of a peptide that emerged over a period of LC elution time in an LC-MS/MS experiment were grouped into a unique mass class (UMC) (38). Each UMC contained all mass spectral features of a peptide, such as charge states, abundances (intensity), scan numbers, and measured monoisotopic masses. Ideally, a peptide is represented by a UMC. For each UMC, the UMC mass was calculated as the intensity-weighted average of the monoisotopic masses of all the UMC components, and the abundance summation of all mass spectral components of the UMC (UMC intensity) was calculated to represent the experimental peptide abundance. During PE-MMR analysis, the precursor masses of the MS/MS spectra (or DTA files) were searched for matches with UMC masses and were replaced by the UMC masses when a match was found. In this process, DTA information was linked to the matched UMC. When the linked DTA file resulted in a peptide sequence with a false positive rate of 1% after SEQUEST searching and target-decoy analysis, the peptide I.D. was recorded in the UMC and the UMC intensity was assigned to the peptide I.D. In this study, normalized elution time (NET) prediction was used to calculate the NETs of the identified UMCs in order to minimize the LC elution time variance of the same peptide across the different LC/MS runs (42).

Construction and Utilization of VAT Master Accurate Mass and Time Tag Database—Information about UMCs with peptide I.D.s from 59 LC-MS/MS data (triplicate LC-MS/MS experiments of 11 samples and 26 LC-MS/MS experiments of OFFGEL fractionations) was compiled into the master accurate mass and time tag (AMT) database (DB) (Oracle Database 10g Enterprise Edition, Release 10.2.0.1.0; Fig. 1*A*).

It is an assembly of AMTs, which are unique peptide sequences whose monoisotopic mass and NET are experimentally determined. When peptides were measured multiple times, the average mass and the median NET were recorded for each AMT.

Due to undersampling of the current proteomic analysis platform, a large portion of UMCs from an LC-MS/MS experiment was not identified in MS/MS experiments and protein database searches. For example, from an individual LC-MS/MS dataset, 87,937 UMCs were measured in MS spectra, and 4,618 of them (approximately 5.3%) were identified by protein database search (identified UMCs; Fig. 1*B*, right top). Peptide ions that were detected in MS scan but with no chance of MS/MS analysis or ions that had undergone fragmentation but with low quality are the main causes of such unidentified UMCs. To assign peptide I.D.s to unidentified UMCs, they were matched to the master AMT DB under mass and NET tolerances (*i.e.* ±10 ppm, ±0.025 NET each; Fig. 1*B*, right bottom). This process of assigning peptide I.D.s to unidentified UMCs resulted in 6,182 additional UMCs identified by the master AMT DB information, making the total number of UMCs with peptide I.D. assignments 10,800 (assigned UMCs).

Alignment of Identified Peptides—After the unidentified UMCs had been assigned with the information from the master AMT DB, the resultant assigned UMCs from the 33 LC-MS/MS datasets (*i.e.* triplicate LC-MS/MS datasets of 11 individual VAT peptide samples) were combined into an alignment table in which each row contained the peptide I.D.s with their corresponding UMC sum intensities from each LC-MS/MS experiment. Quantile normalization of the aligned data was performed to correct the variation in peptide abundance (43) due to variations in the injection amount, and median abundance values of triplicates were obtained. For evaluation of the data reproducibility, similarity scores of two LC-MS/MS runs were measured based on the overlap of detected peptides and their intensity values, as previously described (supplemental Fig. S2) (44). Quantified peptides were rolled up to protein inference by means of bipartite graph analysis (45). The representative protein of each protein group after bipartite graph analysis was set as the protein with the maximum number of unique peptides mapped to a single protein. If two or more proteins in one group had the same number of unique peptides, then the protein with the higher sequence coverage was considered as the representative protein.

Identification of Differentially Expressed Proteins—The intensities of the 22,250 aligned peptides (supplemental Table S2) were normalized using the quantile normalization method (43). From peptide intensities, the relative abundances of corresponding proteins were computed using a linear-programming formulation as described by Dost *et al.* (46). From among the quantified proteins, we selected proteins with at least two nonredundant peptides detected. To identify differentially expressed proteins (DEPs), a $\log_2$ median ratio test was performed to compute the significance of $\log_2$ median ratios for all the proteins (47). An empirical distribution of the null hypothesis (*i.e.* that a protein is not differentially expressed) was estimated by performing hundreds of random permutations of samples and then applying the Gaussian kernel density estimation method to $\log_2$ median ratios resulting from the random permutations (48). FDRs were then computed using the Storey method (49). The DEPs were identified as the ones with an FDR ≤ 0.05 (absolute $\log_2$ fold-changes larger than 1.16, the mean of the 0.25th and 97.5th percentiles of the null distribution).

Enrichment Analysis of GO Biological Processes—Functional enrichment analysis of DEPs was performed using DAVID software (50). GO biological processes enriched by the DEPs were identified as those with $p < 0.05$. We used the p values provided in DAVID.

Reconstruction of Network Model—To reconstruct a network model for DEPs, we first selected a subset of DEPs belonging to GO biological process terms enriched by DEPs and collected their protein–protein interactions from MetaCore™ and four protein–protein interactome databases: BIND (Biomolecular Interaction Network Database) (51), HPRD (Human Protein Reference Database) (52), BioGRID (Biological General Repository for Interaction Datasets) (53), and MINT (Molecular INTeraction Database) (54). The initial network model was built with selected DEPs and their interactions using Cytoscape (55). To incorporate current knowledge into the network, we added proteins involved in immune and metabolic systems and known to contribute to the pathogenesis of metabolic diseases in adipose tissue to the initial network. We then arranged the nodes according to their associated GO biological processes and pathways so that the nodes with similar functions were closely located. A group of nodes involved in the same GO process was labeled with the corresponding GO term.

Western Blot Analysis—For protein confirmation by Western blot, human visceral fat tissue was homogenized in a lysis buffer (Cell Signaling #9803, Danvers, MA) supplemented with protease inhibitors (1 mM phenylmethylsulfonyl fluoride; 100 mM; 2 g/ml aprotinin, 2 g/ml leupeptin). Lipids were eliminated via centrifugation of the solubilized samples at 13,000 rpm for 30 min at 4 °C. The supernatant was collected, and the protein concentration was checked by Bradford assay at 595 nm. Cell lysates (50 μg) were subjected to 10% SDS-PAGE and transferred onto nitrocellulose membranes. The membranes were incubated with primary antibodies. After washing, the blots were incubated with HRP-conjugated secondary antibodies. The blots were developed with Amersham Biosciences solution #RPN2232 and were exposed in a darkroom. The blots were then quantified with Fujifilm Multi Gauge version 3.0. The list of primary antibodies for the selected secretory proteins is summarized in supplemental Table S3.

RESULTS

Comprehensive Global Profiling of VAT Proteome—We first carefully selected drug-naïve T2DM patients ($n = 5$) with diabetes of a short duration (<5 years) and age- and sex-matched subjects with NGT as a control group (see "Experimental Procedures"). Enrolled subjects in this study were all cancer free. The baseline characteristics of T2DM patients and subjects with NGT, such as age, gender, body mass index, disease duration, and other laboratory measures, are summarized in supplemental Table S1. We isolated VATs from elective abdominal surgery for the T2DM patients and normal controls. After removing blood clots, we obtained the lysates of the VATs, removed the lipid layer from the lysates, and then used the filter-aided sample preparation method (25, 56) for protein digestion (see "Experimental Procedures" for details).

To extensively profile the VAT proteome, we generated a master AMT DB (Fig. 1). To this end, we first pooled five normal and five T2DM samples, carried out off-gel fractionation of the pooled proteome into 26 fractions, and analyzed the fractions using ultra-high-pressure nano-LC-MS/MS (Fig. 1*A*). This resulted in 26 LC-MS/MS datasets (supplemental Fig. S3). In addition, we performed triplicate experiments on each of the VATs from five T2DM patients and six subjects with NGT, resulting in 33 LC-MS/MS datasets (supplemental Figs. S4 and S5). A total of 59 LC-MS/MS experiments were used to construct a master AMT DB of the VAT proteome. Briefly, we generated UMCs of peptide MS features from

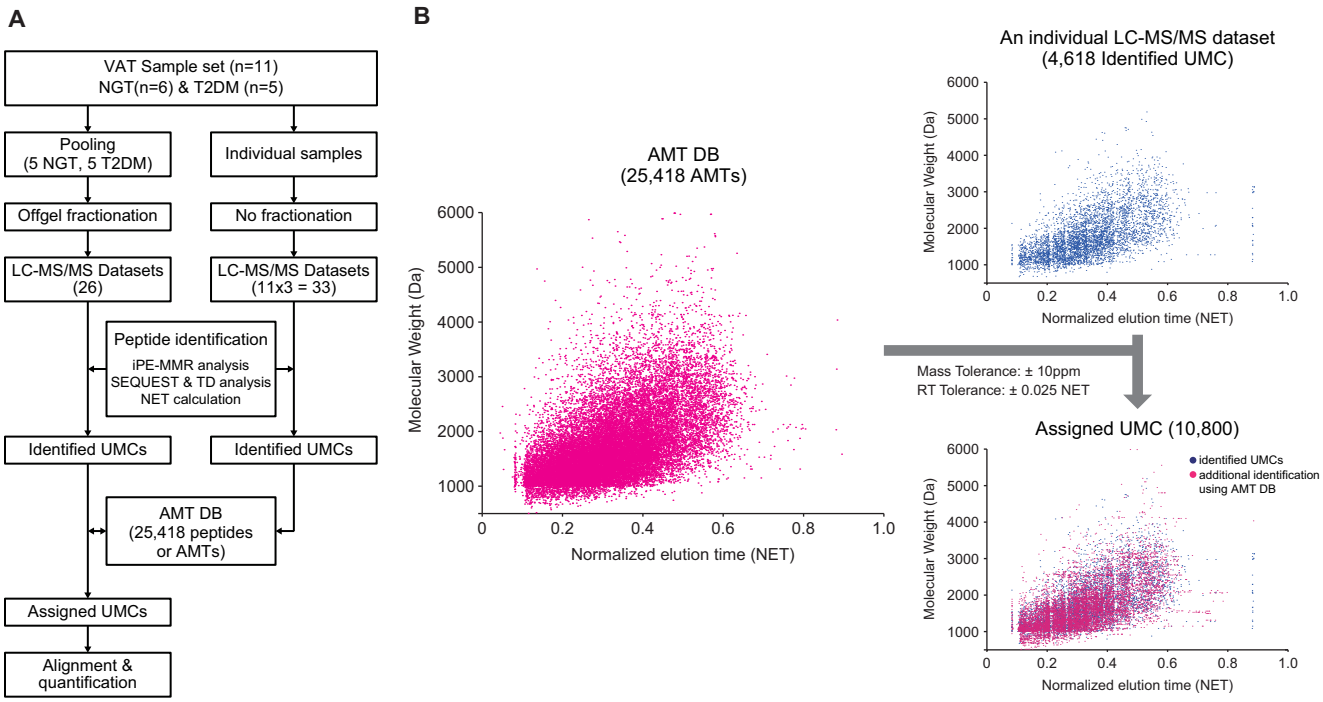

FIG. 1. **The master AMT DB for the VAT proteome.** *A*, the overall scheme of the AMT DB construction. A total of 59 datasets were generated from LC-MS/MS analysis. Each of the 59 datasets was processed by *i*PE-MMR, after which SEQUEST searching was performed. The target-decoy (TD) analysis was performed for the datasets, and then the resultant peptides (or identified UMCs) from both were used to construct the AMT DB (see "Experimental Procedures"). *B*, utilization of AMT DB to assign peptide I.D.s to unidentified UMCs. The 25,418 AMTs (magenta dots) in the AMT DB are visualized in a two-dimensional (NET and molecular weight) scatter plot (left). For an LC-MS/MS dataset, the identified UMCs (blue dots) are shown in the upper-right scatter plot. By matching unidentified UMCs in this dataset with AMTs using the indicated mass and NET tolerances, we assigned a subset of unidentified UMCs with peptide I.D.s of the AMTs matched with them. These matched UMCs are shown in the bottom-right scatter plot.

individual datasets using *i*PE-MMR analysis (36), assigned peptide I.D.s and NETs to UMCs (identified UMCs) after target-decoy SEQUEST search (FDR < 0.01) and NET calculation, respectively, and then compiled all identified UMCs from the 59 datasets into an AMT DB (see "Experimental Procedures" for details). This resulted in a master AMT DB that comprised 25,418 peptides (or AMTs; dots in Fig. 1*B*; supplemental Fig. S6). For each dataset, we then used the master AMT DB to assign peptide I.D.s to unidentified UMCs by matching them with AMTs using the mass and NET tolerances (10 ppm and 0.025 NET, respectively; Fig. 1*B*). From among the 25,418 peptides in the master AMT DB, we selected 22,250 peptides that covered 4,707 VAT proteins with 2 or more sibling peptides and then used them for protein quantitation.

VAT Proteome Profiles Associated with T2DM—To assess the comprehensiveness of our VAT proteome, we first compared the 4,707 proteins detected in VATs (supplemental Table S4) with the adipose proteomes reported in two previous studies (Fig. 2*A*). Xie *et al.* (24) profiled proteomes of SATs, another category of adipose tissue, of three healthy individuals using LC-MS/MS analysis and then identified 1,493 proteins. Adachi *et al.* (23) profiled a proteome of 3T3-L1 adipocytes and then identified 3,287 proteins; this is the most comprehensive adipocyte proteome at present. The comparison showed that 1,089 (73.8% of 1,476) and 1,330 (44.4% of 2,997) gene products were also detected in VATs (Fig. 2*B*). Among the 2,323 genes, 1,542 (66.4%) were detected in at least one of the two studies, and 781 were not detected. These data indicate that our VAT proteome can serve as one of the comprehensive proteomes of adipose tissues.

We then examined cellular processes represented by the 4,707 VAT proteins by performing enrichment analysis of Gene Ontology biological processes (GOBPs) using DAVID software (50). The cellular processes significantly represented by the VAT proteome include the processes related to major functions of adipose tissues, such as oxidation reduction, homeostatic process, inflammatory/immune response, and glucose and lipid metabolic processes (Fig. 2*C*; supplemental Table S5*A*). The enrichment analysis of GO cellular components also revealed that a majority of the VAT proteins were mainly localized in the (i) plasma membrane (21.1%), (ii) cytosol (20.1%), (iii) mitochondrion (15.8%), (iv) extracellular region (14.6%), (v) cytoskeleton (11.2%), (vi) endoplasmic reticulum (8.0%), (vii) vesicle (7.8%), and (viii) Golgi apparatus (5.7%) (Fig. 2*D*; supplemental Table S5*B*). These data indicate that our VAT proteome can provide information related to

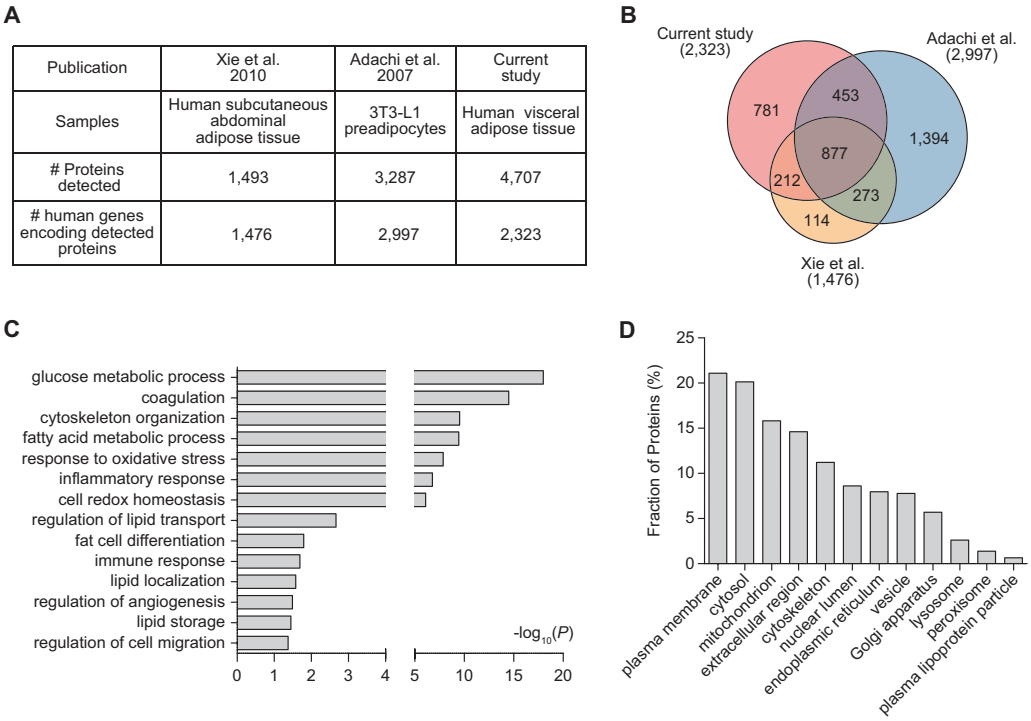

Publication	Xie et al. 2010	Adachi et al. 2007	Current study
Samples	Human subcutaneous abdominal adipose tissue	3T3-L1 preadipocytes	Human visceral adipose tissue
# Proteins detected	1,493	3,287	4,707
# human genes encoding detected proteins	1,476	2,997	2,323

FIG. 2. **Comprehensive proteome of VATs measured from 59 LC-MS/MS analyses.** *A*, comparison of VAT proteome with proteomes previously measured from adipose tissues or cells. The numbers of proteins and genes encoding detected proteins in each study are shown. *B*, Venn diagram showing the relationships of VAT proteome with the adipose proteomes previously reported based on the genes encoding detected proteins in each study. *C*, cellular processes (GOBPs) in which the identified VAT proteins are mainly involved. The bars represent $-\log_{10}(P)$, where P represents the significance of each GOBP being enriched by the VAT proteins. The *p* value was computed by the DAVID software. *D*, relative proportions of Gene Ontology cellular components in which the measured VAT proteins are mainly localized.

diverse functions of adipose tissues occurring in various cellular compartments.

Identification of VAT Proteins Altered in T2DM—To identify VAT proteins whose abundances were altered in T2DM relative to NGT, we first aligned each of 22,250 peptides in the 33 LC-MS/MS datasets (15 for five T2DM patients and 18 for six subjects with NGT) and then determined the ratios of abundances of the 4,707 VAT proteins between T2DM and NGT samples using the linear programming method previously reported (46) (see "Experimental Procedures" for details). Based on the protein ratios, we then identified 772 DEPs (FDR $\leq$ 0.05) between the VATs of subjects with NGT and T2DM ("Experimental Procedures"; supplemental Table S6). Of the 772 DEPs, 444 proteins increased in abundance in T2DM relative to NGT, whereas 328 decreased in T2DM.

To understand the functional association of the DEPs with T2DM, we identified cellular processes represented by the 772 DEPs using DAVID software. This analysis revealed that 444 up-regulated DEPs were mainly involved in inflammatory/immune responses, cytoskeleton organization–related processes (cell migration and cell adhesion), and responses to reactive oxygen species and oxidative stress (Fig. 3*A*; supplemental Table S7*A*), consistent with previous findings recognizing inflammation responses and oxidative stress as major causes of T2DM pathogenesis (1, 57, 58). The 328 down-regulated DEPs were mainly involved in glucose and fatty acid metabolic processes that contribute to T2DM pathogenesis (Fig. 3*B*; supplemental Table S7*B*). A number of studies have demonstrated that the inflammation/immune system and metabolism are highly integrated (58, 59), indicating that the up- and down-regulated DEPs collectively act to define T2DM-related pathophysiology in VATs.

To explore the collective function of these T2DM-related processes, we reconstructed network models describing the interactions among the DEPs involved in the processes represented by the 444 up-regulated DEPs (Fig. 3*C*) and the 328 down-regulated DEPs (Fig. 3*D*). The DEPs in these network models were grouped into functional modules, each of which included the DEPs involved in the corresponding GOBP shown in Figs. 3*A* and 3*B*. Several modules, including complement cascade, inflammatory/immune response, and ECM-receptor interaction, showed dense interactions within themselves and between one another through transcription factors (NFKB1/RELA, STAT3, and STAT5B) (Fig. 3*C*). Also, significant numbers of molecules involved in metabolic pathways (pyruvate metabolism, tricarboxylic acid cycle, OXPHOS, and fatty acid β-oxidation) were decreased in T2DM (Fig. 3*D*).

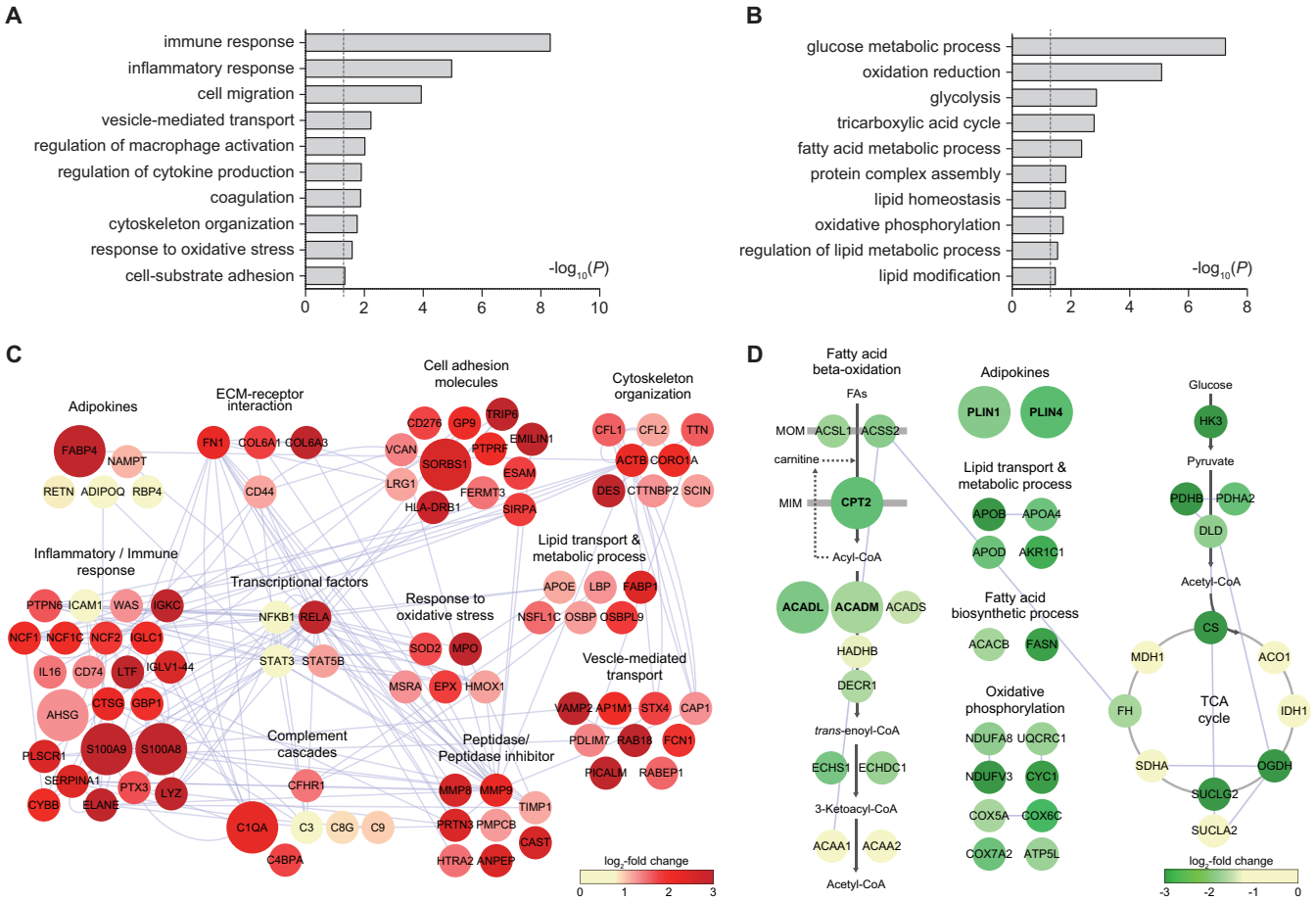

FIG. 3. **Network models delineating cellular processes represented by type 2 diabetes–related VAT proteins (DEPs).** *A*, *B*, cellular processes (GOBPs) represented by the up-regulated (*A*) and down-regulated (*B*) proteins. The bars represent $-\log_{10}(P)$, where P represents the significance of each GOBP being enriched by the DEPs. *C*, *D*, network models describing the GOBPs represented by the up-regulated (*C*) and down-regulated (*D*) proteins. Node colors represent the increase (red) and the decrease (green) in the abundance of VAT proteins in T2DM samples relative to normal controls. The color bar denotes the gradient of $\log_2$-fold changes. Edges represent protein–protein interactions (gray) collected from five interactome databases (see "Experimental Procedures") and metabolic reactions (arrows) obtained from the KEGG pathway database. See "Experimental Procedures" for grouping of the nodes in the network.

These data indicate a collective contribution of these modules and pathways to T2DM pathogenesis.

A Proteome Profile Representing the Pathophysiology of VAT—VATs in T2DM are characterized by chronic inflammation and metabolic alterations (57–59). Consistently, the network models showed alterations of the processes related to inflammation (Fig. 3*C*) and metabolism (Fig. 3*D*) in T2DM VATs. Thus, to select a proteome profile that could represent the collective pathophysiology of VATs in T2DM, we focused on the DEPs that were involved in these processes. Furthermore, VAT is an endocrine organ secreting a wide range of molecules (1). The DEPs that are secreted from VATs can alter the processes related to inflammation and metabolism (1, 60). Among the 772 DEPs, we thus identified 320 proteins (163 genes) that can be secreted from VATs using the GO cellular component information (*i.e.* extracellular region) and the Human Plasma Proteome Project data (supplemental Table S8) (61). Using the network models and/or the secretory proteins, we selected a proteome profile that could represent the alterations in the processes related to inflammation and metabolism as described in supplemental Fig. S7. First, for the inflammation-related processes in the network model, we focused on 21 secretory DEPs involved in the three inflammation-related modules of inflammatory/immune response, complement cascade, and cell adhesion in the network model (Fig. 3*C*; supplemental Fig. S7). From among these, we selected the following five proteins that can represent the alterations of the processes corresponding to the network modules: α-2-HS-glycoprotein and S100 calcium binding protein A8/9 (S100A8/9; Calprotectin) for the inflammatory/immune response module; complement component 1, q subcomponent, A chain (C1QA) for the complement cascade module; and sorbin and SH3 domain containing 1 (SORBS1) for the cell adhesion module. Second, for the metabolism-related processes in the network model, we focused on seven DEPs involved in the pathway of fatty acid β-oxidation, which is

more relevant to adipose tissue than the glycolytic pathway, in the network model (Fig. 3*D*). From among them, we selected three metabolic enzymes, carnitine palmitoyltransferase 2, acyl-CoA dehydrogenase, long chain (ACADL), and acyl-CoA dehydrogenase, C-4 to C-12 straight chain (ACADM) (supplemental Fig. S7). Third, adipokines are the most well-known class of proteins secreted from adipose tissue, which can affect both inflammation and metabolic alterations in T2DM VATs. Interestingly, the 320 secretory DEPs included the three adipokines fatty acid binding protein 4 (FABP4) and perilipin 1 and 4 (PLIN1 and PLIN4). Thus, we selected additionally these three adipokines. A total of 11 proteins were selected as a protein profile that could represent the pathophysiology of VAT in the early pathogenesis of T2DM.

Validation of the Selected Protein Profile—To test the validity of the 11 selected proteins, we collected the VATs from an independent set of 10 early T2DM patients and 10 subjects with NGT based on the same criteria ("Experimental Procedures") employed for the collection of the samples at the discovery phase using LC-MS/MS analysis (supplemental Table S1). In these new samples, using Western blotting, we then tested the differential expression of the 11 selected proteins measured by LC-MS/MS analysis (*i.e.* up-regulation of FABP4, S100A8/9, SORBS1, α-2-HS-glycoprotein, and C1QA and down-regulation of PLIN1/4, carnitine palmitoyltransferase 2, ACADL, and ACADM in T2DM relative to NGT; 11 proteins in red in supplemental Fig. S7). From among the 11 selected proteins, we finally selected the six proteins that showed significant changes in the independent samples consistent with those shown in the LC-MS/MS data (Figs. 4*A* and 4*B*, supplemental Fig. S8). Finally, we assessed whether the six proteins could be used to monitor the pathophysiology of VATs in T2DM. To this end, we quantified the abundances of the six proteins from the results of Western blotting and then evaluated whether their abundances were capable of distinguishing T2DM patients from subjects with NGT using partial least square discriminant analysis (Fig. 4*C*) (41). Nine out of the 10 T2DM samples were correctly separated from the 10 NGT controls. Taken together, these data indicate that the six proteins can be used as a protein profile that represents the pathophysiology of VAT in the early pathogenesis of T2DM.

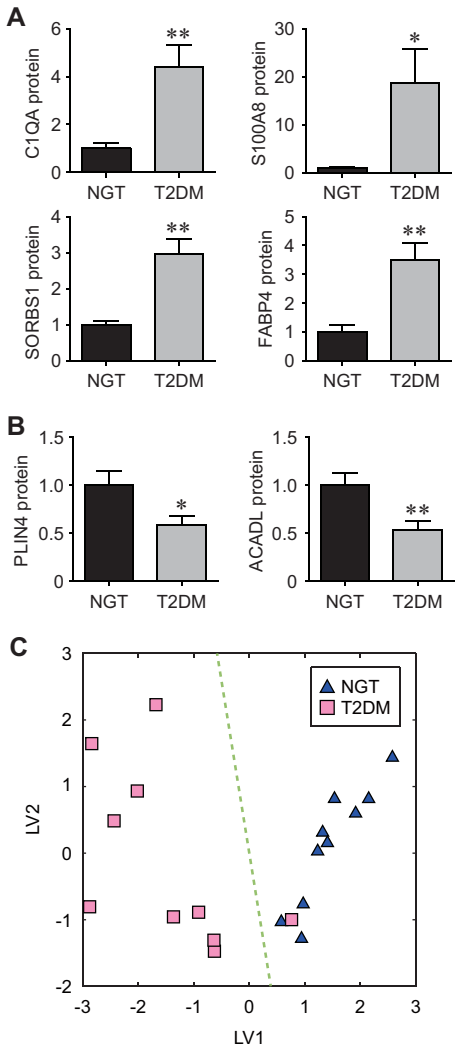

FIG. 4. **Validation of the selected VAT proteins.** *A*, *B*, Western blotting analysis of the selected VAT proteins in the independent set of VAT samples obtained from T2DM patients and subjects with NGT. Up-regulation of FABP4, C1QA, S100A8, and SORBS1 and down-regulation of ACADL and PLIN4 in VAT samples of T2DM patients were confirmed. The data are shown as mean ± S.D. $^{*}p < 0.05$, $^{**}p < 0.01$ by Student's *t* test. *C*, partial least square discriminant analysis showing that the confirmed six VAT proteins can achieve clear separation between T2DM and NGT samples. The green line indicates a decision function between T2DM and NGT samples. LV1 and LV2 represent the first and second latent variables identified by partial least square discriminant analysis. The coordinates of each sample in the LV1–LV2 space were computed by projecting the amounts of the six VAT proteins onto LV1 and LV2.

DISCUSSION

Visceral fat accumulation is a key feature of chronic metabolic diseases related to lipotoxicity, such as diabetes, metabolic syndrome, obesity, and cardiovascular disease. Metabolic and functional disruption in adipose tissue can serve as an essential dimension of molecular signatures that can be used to understand the pathogenesis of T2DM. However, the alteration of these signatures in VATs has been considered clinically important but has not been systematically explored. In this study, we thus examined comprehensive proteome profiles of VATs to identify a proteome profile representing key pathophysiological features of VATs, inflammation of adipose tissue and metabolic alteration, linked to the pathogenesis of T2DM. To achieve this goal, we developed an approach that involved (i) comprehensive proteome profiling of whole VATs with removal of blood clots and lipid layers from the lysates, generation of a master AMT DB, and ultra-high-pressure nano-LC-MS/MS analysis; (ii) identification of DEPs in the VATs collected from subjects with T2DM and NGT; (iii) the selection of a protein profile able to represent the T2DM-

related pathophysiology of VATs by integrating T2DM-related network models of VATs and functions of the proteome secreted from VATs; and (iv) validation of the selected protein profile in independent T2DM using Western blotting and confirmation of the validated protein profile able to distinguish T2DM samples from NGT controls by means of partial least square discriminant analysis. Using this approach, we identified a protein profile composed of six VAT proteins (three up-regulated and inflammation-related (S100A8, C1QA, and SORBS1), one down-regulated and metabolism-related (ACADL), and two adipokines (FABP4 and PLIN4)).

A number of previous studies have shown associations of the six proteins selected in this study with T2DM in various systems (*e.g.* serum/plasma, urine, muscle, or liver; supplemental Table S9). A higher serum FABP4 level was linked to obesity, insulin resistance, and T2DM (62, 63). The amount of the serum C1q-adiponectin complex showed a significant correlation with coronary artery disease in Japanese T2DM subjects (64). The amounts of S100A8/9 (calprotectin) in both urine and plasma were associated with chronic low-grade inflammation and insulin resistance (65, 66), and mRNA levels of S100A8 were elevated in the adipocyte fraction of obese mice (67). SORBS1(CAP) blocks the stimulation of glucose transport by insulin in 3T3-L1 adipocytes (68), and the T228A polymorphism of SORBS1 was linked to both obesity and diabetes (69). ACADL knockout mice showed increased triglyceride storage in both muscle and liver and severe hepatic insulin resistance (70). The 11482G→A polymorphism of the PLIN4 gene was associated with a higher risk of obesity and metabolic syndrome (71). However, none of these proteins have been previously reported to be altered in their protein levels in human adipose tissue or VATs of early T2DM relative to normal controls (supplemental Table S9). Note that the mRNA levels of S100A8/9 were elevated in the mouse adipocyte fraction. These data indicate two aspects of the six-protein panel: (i) the alterations of mRNA or protein levels of these proteins in other systems suggest the validity of the six proteins as a protein profile that can represent the pathophysiology of T2DM VATs; and (ii) the fact that no alterations of these proteins in protein levels were previously shown in human adipose tissue or VAT suggests the novelty of the six-protein panel.

Previously, Xie *et al.* and Adachi *et al.* provided the proteomes of abdominal SATs of healthy individuals and mouse 3T3-L1 adipocytes, respectively (supplemental Table S9). Although these datasets could have served as useful resources for various studies of adipose-related diseases, neither study compared the proteomes with those in T2DM, and thus they provide no lists of DEPs in T2DM relative to normal controls. Four of the six proteins were detected in either of these studies, but alterations of their abundances in T2DM have remained unknown. Also, several studies (18, 19, 72, 73) have included comparative proteomic analyses in muscle, salivary, serum, and pancreatic islet tissues, providing the proteomes and lists of DEPs in these tissues collected from T2DM patients or mice relative to controls (supplemental Table S9). Among the six proteins, three (S100A8, C1QA, and FABP4) have been detected in one of these tissues, but only C1QA showed alteration in its protein abundance in T2DM serum. Nonetheless, none of the six proteins selected in this study have been previously reported to be altered in protein levels in human adipose tissue or VATs in early T2DM.

Taken as a whole, our study showed for the first time the differential expression of six selected proteins that have been previously linked to T2DM pathogenesis in other systems in VATs of early T2DM patients, thereby supporting their potential use as indicators of the early pathogenesis of T2DM. The clinical implications of the six selected proteins can be further tested with a larger number of early T2DM patients. In addition, longitudinal studies can be designed to further demonstrate the nature of dynamic changes of the proposed protein profile during the course of T2DM pathogenesis. Also, novel subtypes of early, drug-naïve T2DM patients might be further characterized based on the dimension of inflammation of adipose tissue and metabolic changes in VATs represented by the proposed protein profile.

The six selected VAT proteins correctly distinguished 90% of T2DM patients from subjects with NGT, suggesting the potential use of the selected proteome profile in understanding the pathophysiological states of T2DM (Fig. 4*C*). One T2DM sample was classified into NGTs. We carefully examined clinical characteristics of this patient and compared them with those of the other T2DM patients. Disease duration, diabetes mellitus status, and management of this outlier patient were similar to those of the other T2DM patients. However, this patient was the oldest man in our test set and had taken antihypertensive medication for more than 4 years. The patient's age of 75 (mean age = 66.8 in the test set), survivor deviation, and the history of hypertension could have induced the difference between this patient and the other T2DM patients, and/or the antihypertensive medication could have made the profile of the six selected DEPs in this patient similar to those in NGTs. However, more detailed functional studies should be carried out to elucidate the mechanisms underlying the similarity in the profiles of the six selected DEPs between this patient and NGTs.

In addition to the six proteins selected in this study, our approach provided a comprehensive list of DEPs or secretory proteins in VATs in early T2DM pathogenesis, thus extending extensively the current list identified by conventional small-scale experiments or approaches (supplemental Table S6). This list of proteins can serve as a comprehensive resource for biologists who study adipose tissue and interactions among the cells constituting VATs based on the DEPs and secretory proteins, respectively. Furthermore, the network models can provide a basis for understanding inflammation of adipose tissue (Fig. 3*C*) and metabolic alterations in VATs during the early pathogenesis of T2DM (Fig. 3*D*). The network

models further suggested that fatty acid oxidation, insulin signaling, adipose tissue inflammation, and PPARγ pathways associated with the DEPs should be involved in early pathophysiological changes of VATs in T2DM. This understanding can further suggest proactive therapeutic options involving antidiabetic treatments during the early pathogenesis of T2DM. In summary, our approach successfully identified a protein profile that can provide a novel dimension of information indicative of T2DM for the classification, therapy, and pathogenesis of T2DM.

Acknowledgments—We thank Mi Hong Ji for her technical assistance.

* This study was supported by Korea Health 21 R&D Project grants (A111218-11-CP02 from the National Project for Personalized Genomic Medicine), Korean MEST grants (Proteogenomics Project; Converging Research Center Program, 2013K000443; Priority Research Centers Program, NRF20100020209; Institute for Basic Science, CA1308), the POSCO Research Fund (Project No. 2013Y008), and a Korea University Grant.

[S] This article contains supplemental material.

§§ To whom correspondence should be addressed: Daehee Hwang, Ph.D., Department of New Biology, DGIST, 50-1, Sang-Ri, Hyeonpung-Myeon, Dalseong-Gun, Daegu 711-873, Republic of Korea, Tel.: 82-53-785-1840, Fax: 82-53-785-1819, E-mail: dhwang@dgist.ac.kr; Sung Hee Choi, M.D., Ph.D., Seoul National University, Bundang Hospital, Internal Medicine, Endocrinology and Metabolism, Seoul National University College of Medicine, Gumidong 300, Bundang, Seongnam, Gyeonggi-do, 463-707, Republic of Korea, Tel.: 82-31-787-7033, Fax: 82-31-787-4052, E-mail: drshchoi@snu.ac.kr; Sang-Won Lee, Ph.D., Department of Chemistry, Korea University, 1, 5-ka, Anam-dong, Seongbuk-gu, Seoul, 136-701, Republic of Korea, Tel.: 82-2-3290-3603, Fax: 82-2-3290-3121, E-mail: sw_lee@korea.ac.kr.

¶ These authors contributed to this work equally.

REFERENCES

1. Hajer, G. R., van Haeften, T. W., and Visseren, F. L. (2008) Adipose tissue dysfunction in obesity, diabetes, and vascular diseases. *Eur. Heart J.* **29,** 2959–2971
2. Riordan, N. H., Ichim, T. E., Min, W. P., Wang, H., Solano, F., Lara, F., Alfaro, M., Rodriguez, J. P., Harman, R. J., Patel, A. N., Murphy, M. P., Lee, R. R., and Minev, B. (2009) Non-expanded adipose stromal vascular fraction cell therapy for multiple sclerosis. *J. Translat. Med.* **7,** 29
3. Ibrahim, M. M. (2010) Subcutaneous and visceral adipose tissue: structural and functional differences. *Obesity Rev.* **11,** 11–18
4. Bjorndal, B., Burri, L., Staalesen, V., Skorve, J., and Berge, R. K. (2011) Different adipose depots: their role in the development of metabolic syndrome and mitochondrial response to hypolipidemic agents. *J. Obesity* **2011,** 490650
5. Schernthaner, G. H., and Schernthaner, G. (2005) Insulin resistance and inflammation in the early phase of type 2 diabetes: potential for therapeutic intervention. *Scand. J. Clin. Lab. Invest.* **240,** 30–40
6. Peral, B., Camafeita, E., Fernandez-Real, J. M., and Lopez, J. A. (2009) Tackling the human adipose tissue proteome to gain insight into obesity and related pathologies. *Expert Rev. Proteomics* **6,** 353–361
7. Kishida, K., Funahashi, T., Matsuzawa, Y., and Shimomura, I. (2012) Visceral adiposity as a target for the management of the metabolic syndrome. *Ann. Med.* **44,** 233–241
8. Duvnjak, L., and Duvnjak, M. (2009) The metabolic syndrome—an ongoing story. *J. Physiol. Pharmacol.* **60 Suppl 7,** 19–24
9. Boden, G. (2003) Effects of free fatty acids (FFA) on glucose metabolism: significance for insulin resistance and type 2 diabetes. *Exp. Clin. Endocrinol. Diabetes* **111,** 121–124
10. Rytka, J. M., Wueest, S., Schoenle, E. J., and Konrad, D. (2011) The portal theory supported by venous drainage-selective fat transplantation. *Diabetes* **60,** 56–63
11. Ozcelik, F., Yuksel, C., Arslan, E., Genc, S., Omer, B., and Serdar, M. A. (2013) Relationship between visceral adipose tissue and adiponectin, inflammatory markers and thyroid hormones in obese males with hepatosteatosis and insulin resistance. *Arch. Med. Res.* **44,** 273–280
12. Lehr, S., Hartwig, S., Lamers, D., Famulla, S., Muller, S., Hanisch, F. G., Cuvelier, C., Ruige, J., Eckardt, K., Ouwens, D. M., Sell, H., and Eckel, J. (2012) Identification and validation of novel adipokines released from primary human adipocytes. *Mol. Cell. Proteomics* **11,** M111.010504
13. Gastaldelli, A., Miyazaki, Y., Pettiti, M., Matsuda, M., Mahankali, S., Santini, E., DeFronzo, R. A., and Ferrannini, E. (2002) Metabolic effects of visceral fat accumulation in type 2 diabetes. *J. Clin. Endocrinol. Metab.* **87,** 5098–5103
14. Frayn, K. N. (2000) Visceral fat and insulin resistance—causative or correlative? *Br. J. Nutrition* **83 Suppl 1,** S71–S77
15. Fontana, L., Eagon, J. C., Trujillo, M. E., Scherer, P. E., and Klein, S. (2007) Visceral fat adipokine secretion is associated with systemic inflammation in obese humans. *Diabetes* **56,** 1010–1013
16. Miyazaki, Y., Glass, L., Triplitt, C., Wajcberg, E., Mandarino, L. J., and DeFronzo, R. A. (2002) Abdominal fat distribution and peripheral and hepatic insulin resistance in type 2 diabetes mellitus. *Am. J. Physiol. Endocrinol. Metab.* **283,** E1135–E1143
17. Despres, J. P., and Lemieux, I. (2006) Abdominal obesity and metabolic syndrome. *Nature* **444,** 881–887
18. Li, R. X., Chen, H. B., Tu, K., Zhao, S. L., Zhou, H., Li, S. J., Dai, J., Li, Q. R., Nie, S., Li, Y. X., Jia, W. P., Zeng, R., and Wu, J. R. (2008) Localized-statistical quantification of human serum proteome associated with type 2 diabetes. *PLoS One* **3,** e3224
19. Rao, P. V., Reddy, A. P., Lu, X., Dasari, S., Krishnaprasad, A., Biggs, E., Roberts, C. T., and Nagalla, S. R. (2009) Proteomic identification of salivary biomarkers of type-2 diabetes. *J. Proteome Res.* **8,** 239–245
20. Sundsten, T., Eberhardson, M., Goransson, M., and Bergsten, P. (2006) The use of proteomics in identifying differentially expressed serum proteins in humans with type 2 diabetes. *Proteome Sci.* **4,** 22
21. Sanchez, J. C., Converset, V., Nolan, A., Schmid, G., Wang, S., Heller, M., Sennitt, M. V., Hochstrasser, D. F., and Cawthorne, M. A. (2002) Effect of rosiglitazone on the differential expression of diabetes-associated proteins in pancreatic islets of C57Bl/6 lep/lep mice. *Mol. Cell. Proteomics* **1,** 509–516
22. Hojlund, K., Wrzesinski, K., Larsen, P. M., Fey, S. J., Roepstorff, P., Handberg, A., Dela, F., Vinten, J., McCormack, J. G., Reynet, C., and Beck-Nielsen, H. (2003) Proteome analysis reveals phosphorylation of ATP synthase beta-subunit in human skeletal muscle and proteins with potential roles in type 2 diabetes. *J. Biol. Chem.* **278,** 10436–10442
23. Adachi, J., Kumar, C., Zhang, Y., and Mann, M. (2007) In-depth analysis of the adipocyte proteome by mass spectrometry and bioinformatics. *Mol. Cell. Proteomics* **6,** 1257–1273
24. Xie, X., Yi, Z., Bowen, B., Wolf, C., Flynn, C. R., Sinha, S., Mandarino, L. J., and Meyer, C. (2010) Characterization of the human adipocyte proteome and reproducibility of protein abundance by one-dimensional gel electrophoresis and HPLC-ESI-MS/MS. *J. Proteome Res.* **9,** 4521–4534
25. Wisniewski, J. R., Zougman, A., Nagaraj, N., and Mann, M. (2009) Universal sample preparation method for proteome analysis. *Nat. Methods* **6,** 359–362
26. International Expert Committee (2009) International Expert Committee report on the role of the A1C assay in the diagnosis of diabetes. *Diabetes Care* **32,** 1327–1334
27. Peinado, J. R., Jimenez-Gomez, Y., Pulido, M. R., Ortega-Bellido, M., Diaz-Lopez, C., Padillo, F. J., Lopez-Miranda, J., Vazquez-Martinez, R., and Malagon, M. M. (2010) The stromal-vascular fraction of adipose tissue contributes to major differences between subcutaneous and visceral fat depots. *Proteomics* **10,** 3356–3366
28. Mastro, R., and Hall, M. (1999) Protein delipidation and precipitation by tri-n-butylphosphate, acetone, and methanol treatment for isoelectric focusing and two-dimensional gel electrophoresis. *Anal. Biochem.* **273,** 313–315
29. Peinado, J. R., Pardo, M., de la Rosa, O., and Malagon, M. M. (2012) Proteomic characterization of adipose tissue constituents, a necessary step for understanding adipose tissue complexity. *Proteomics* **12,**

607–620
30. Corton, M., Villuendas, G., Botella, J. I., San Millan, J. L., Escobar-Morreale, H. F., and Peral, B. (2004) Improved resolution of the human adipose tissue proteome at alkaline and wide range pH by the addition of hydroxyethyl disulfide. *Proteomics* **4,** 438–441
31. Yu, Y. Q., Gilar, M., Lee, P. J., Bouvier, E. S., and Gebler, J. C. (2003) Enzyme-friendly, mass spectrometry-compatible surfactant for in-solution enzymatic digestion of proteins. *Anal. Chem.* **75,** 6023–6028
32. Horth, P., Miller, C. A., Preckel, T., and Wenz, C. (2006) Efficient fractionation and improved protein identification by peptide OFFGEL electrophoresis. *Mol. Cell. Proteomics* **5,** 1968–1974
33. Lee, J. H., Hyung, S. W., Mun, D. G., Jung, H. J., Kim, H., Lee, H., Kim, S. J., Park, K. S., Moore, R. J., Smith, R. D., and Lee, S. W. (2012) Fully automated multifunctional ultrahigh pressure liquid chromatography system for advanced proteome analyses. *J. Proteome Res.* **11,** 4373–4381
34. Hyung, S. W., Kim, M. S., Mun, D. G., Lee, H., and Lee, S. W. (2011) The effect and potential of using a temperature controlled separation column with ultra-high pressure microcapillary liquid chromatography/tandem mass spectrometry on proteomic analysis. *Analyst* **136,** 2100–2105
35. Kelly, R. T., Page, J. S., Tang, K., and Smith, R. D. (2007) Array of chemically etched fused-silica emitters for improving the sensitivity and quantitation of electrospray ionization mass spectrometry. *Anal. Chem.* **79,** 4192–4198
36. Jung, H. J., Purvine, S. O., Kim, H., Petyuk, V. A., Hyung, S. W., Monroe, M. E., Mun, D. G., Kim, K. C., Park, J. M., Kim, S. J., Tolic, N., Slysz, G. W., Moore, R. J., Zhao, R., Adkins, J. N., Anderson, G. A., Lee, H., Camp, D. G., 2nd, Yu, M. H., Smith, R. D., and Lee, S. W. (2010) Integrated post-experiment monoisotopic mass refinement: an integrated approach to accurately assign monoisotopic precursor masses to tandem mass spectrometric data. *Anal. Chem.* **82,** 8510–8518
37. Mayampurath, A. M., Jaitly, N., Purvine, S. O., Monroe, M. E., Auberry, K. J., Adkins, J. N., and Smith, R. D. (2008) DeconMSn: a software tool for accurate parent ion monoisotopic mass determination for tandem mass spectra. *Bioinformatics* **24,** 1021–1023
38. Shin, B., Jung, H. J., Hyung, S. W., Kim, H., Lee, D., Lee, C., Yu, M. H., and Lee, S. W. (2008) Postexperiment monoisotopic mass filtering and refinement (PE-MMR) of tandem mass spectrometric data increases accuracy of peptide identification in LC/MS/MS. *Mol. Cell. Proteomics* **7,** 1124–1134
39. Petyuk, V. A., Jaitly, N., Moore, R. J., Ding, J., Metz, T. O., Tang, K., Monroe, M. E., Tolmachev, A. V., Adkins, J. N., Belov, M. E., Dabney, A. R., Qian, W. J., Camp, D. G., 2nd, and Smith, R. D. (2008) Elimination of systematic mass measurement errors in liquid chromatography-mass spectrometry based proteomics using regression models and a priori partial knowledge of the sample content. *Anal. Chem.* **80**, 693–706
40. Petyuk, V. A., Mayampurath, A. M., Monroe, M. E., Polpitiya, A. D., Purvine, S. O., Anderson, G. A., Camp, D. G., 2nd, and Smith, R. D. (2010) DtaRefinery, a software tool for elimination of systematic errors from parent ion mass measurements in tandem mass spectra data sets. *Mol. Cell. Proteomics* **9**, 486–496
41. Hyung, S. W., Lee, M. Y., Yu, J. H., Shin, B., Jung, H. J., Park, J. M., Han, W., Lee, K. M., Moon, H. G., Zhang, H., Aebersold, R., Hwang, D., Lee, S. W., Yu, M. H., and Noh, D. Y. (2011) A serum protein profile predictive of the resistance to neoadjuvant chemotherapy in advanced breast cancers. *Mol. Cell. Proteomics* **10,** M111.011023
42. Jaitly, N., Monroe, M. E., Petyuk, V. A., Clauss, T. R., Adkins, J. N., and Smith, R. D. (2006) Robust algorithm for alignment of liquid chromatography-mass spectrometry analyses in an accurate mass and time tag data analysis pipeline. *Anal. Chem.* **78,** 7397–7409
43. Bolstad, B. M., Irizarry, R. A., Astrand, M., and Speed, T. P. (2003) A comparison of normalization methods for high density oligonucleotide array data based on variance and bias. *Bioinformatics* **19,** 185–193
44. Mueller, L. N., Rinner, O., Schmidt, A., Letarte, S., Bodenmiller, B., Brusniak, M. Y., Vitek, O., Aebersold, R., and Muller, M. (2007) SuperHirn—a novel tool for high resolution LC-MS-based peptide/protein profiling. *Proteomics* **7,** 3470–3480
45. Zhang, B., Chambers, M. C., and Tabb, D. L. (2007) Proteomic parsimony through bipartite graph analysis improves accuracy and transparency. *J. Proteome Res.* **6,** 3549–3557
46. Dost, B., Bandeira, N., Li, X., Shen, Z., Briggs, S. P., and Bafna, V. (2012) Accurate mass spectrometry based protein quantification via shared peptides. *J. Comput. Biol.* **19,** 337–348
47. Lee, H. J., Suk, J. E., Patrick, C., Bae, E. J., Cho, J. H., Rho, S., Hwang, D., Masliah, E., and Lee, S. J. (2010) Direct transfer of alpha-synuclein from neuron to astroglia causes inflammatory responses in synucleinopathies. *J. Biol. Chem.* **285,** 9262–9272
48. Bowman, A. W., and Azzalini, A. (1997) *Applied Smoothing Techniques for Data Analysis: The Kernel Approach with S-Plus Illustrations*, Clarendon Press/Oxford University Press, Oxford, UK
49. Storey, J. D., and Tibshirani, R. (2003) Statistical significance for genome-wide studies. *Proc. Natl. Acad. Sci. U.S.A.* **100,** 9440–9445
50. Huang da, W., Sherman, B. T., and Lempicki, R. A. (2009) Systematic and integrative analysis of large gene lists using DAVID bioinformatics resources. *Nat. Protoc.* **4,** 44–57
51. Bader, G. D., Betel, D., and Hogue, C. W. (2003) BIND: the Biomolecular Interaction Network Database. *Nucleic Acids Res.* **31,** 248–250
52. Peri, S., Navarro, J. D., Kristiansen, T. Z., Amanchy, R., Surendranath, V., Muthusamy, B., Gandhi, T. K., Chandrika, K. N., Deshpande, N., Suresh, S., Rashmi, B. P., Shanker, K., Padma, N., Niranjan, V., Harsha, H. C., Talreja, N., Vrushabendra, B. M., Ramya, M. A., Yatish, A. J., Joy, M., Shivashankar, H. N., Kavitha, M. P., Menezes, M., Choudhury, D. R., Ghosh, N., Saravana, R., Chandran, S., Mohan, S., Jonnalagadda, C. K., Prasad, C. K., Kumar-Sinha, C., Deshpande, K. S., and Pandey, A. (2004) Human protein reference database as a discovery resource for proteomics. *Nucleic Acids Res.* **32,** D497–D501
53. Stark, C., Breitkreutz, B. J., Reguly, T., Boucher, L., Breitkreutz, A., and Tyers, M. (2006) BioGRID: a general repository for interaction datasets. *Nucleic Acids Res.* **34,** D535–D539
54. Chatr-aryamontri, A., Ceol, A., Palazzi, L. M., Nardelli, G., Schneider, M. V., Castagnoli, L., and Cesareni, G. (2007) MINT: the Molecular INTeraction database. *Nucleic Acids Res.* **35,** D572–D574
55. Cline, M. S., Smoot, M., Cerami, E., Kuchinsky, A., Landys, N., Workman, C., Christmas, R., Avila-Campilo, I., Creech, M., Gross, B., Hanspers, K., Isserlin, R., Kelley, R., Killcoyne, S., Lotia, S., Maere, S., Morris, J., Ono, K., Pavlovic, V., Pico, A. R., Vailaya, A., Wang, P. L., Adler, A., Conklin, B. R., Hood, L., Kuiper, M., Sander, C., Schmulevich, I., Schwikowski, B., Warner, G. J., Ideker, T., and Bader, G. D. (2007) Integration of biological networks and gene expression data using Cytoscape. *Nat. Protoc.* **2,** 2366–2382
56. Zielinska, D. F., Gnad, F., Wisniewski, J. R., and Mann, M. (2010) Precision mapping of an in vivo N-glycoproteome reveals rigid topological and sequence constraints. *Cell* **141,** 897–907
57. Guilherme, A., Virbasius, J. V., Puri, V., and Czech, M. P. (2008) Adipocyte dysfunctions linking obesity to insulin resistance and type 2 diabetes. *Nat. Rev. Mol. Cell Biol.* **9,** 367–377
58. Tilg, H., and Moschen, A. R. (2006) Adipocytokines: mediators linking adipose tissue, inflammation and immunity. *Nat. Rev. Immunol.* **6,** 772–783
59. Osborn, O., and Olefsky, J. M. (2012) The cellular and signaling networks linking the immune system and metabolism in disease. *Nat. Med.* **18,** 363–374
60. Wozniak, S. E., Gee, L. L., Wachtel, M. S., and Frezza, E. E. (2009) Adipose tissue: the new endocrine organ? A review article. *Digestive Dis. Sci.* **54,** 1847–1856
61. Farrah, T., Deutsch, E. W., Omenn, G. S., Campbell, D. S., Sun, Z., Bletz, J. A., Mallick, P., Katz, J. E., Malmstrom, J., Ossola, R., Watts, J. D., Lin, B., Zhang, H., Moritz, R. L., and Aebersold, R. (2011) A high-confidence human plasma proteome reference set with estimated concentrations in PeptideAtlas. *Mol. Cell. Proteomics* **10,** M110.006353
62. Cabre, A., Lazaro, I., Girona, J., Manzanares, J. M., Marimon, F., Plana, N., Heras, M., and Masana, L. (2007) Fatty acid binding protein 4 is increased in metabolic syndrome and with thiazolidinedione treatment in diabetic patients. *Atherosclerosis* **195,** e150–e158
63. Cabre, A., Lazaro, I., Girona, J., Manzanares, J. M., Marimon, F., Plana, N., Heras, M., and Masana, L. (2008) Plasma fatty acid-binding protein 4 increases with renal dysfunction in type 2 diabetic patients without microalbuminuria. *Clin. Chem.* **54,** 181–187
64. Hirata, A., Kishida, K., Nakatsuji, H., Kobayashi, H., Funahashi, T., and Shimomura, I. (2013) High serum C1q-adiponectin/total adiponectin ratio correlates with coronary artery disease in Japanese type 2 diabetics. *Metab. Clin. Exp.* **62,** 578–585
65. Ortega, F. J., Sabater, M., Moreno-Navarrete, J. M., Pueyo, N., Botas, P.,

Delgado, E., Ricart, W., Fruhbeck, G., and Fernandez-Real, J. M. (2012) Serum and urinary concentrations of calprotectin as markers of insulin resistance and type 2 diabetes. *Eur. J. Endocrinol.* **167,** 569–578

66. Mortensen, O. H., Nielsen, A. R., Erikstrup, C., Plomgaard, P., Fischer, C. P., Krogh-Madsen, R., Lindegaard, B., Petersen, A. M., Taudorf, S., and Pedersen, B. K. (2009) Calprotectin—a novel marker of obesity. *PLoS One* **4,** e7419
67. Sekimoto, R., Kishida, K., Nakatsuji, H., Nakagawa, T., Funahashi, T., and Shimomura, I. (2012) High circulating levels of S100A8/A9 complex (calprotectin) in male Japanese with abdominal adiposity and dysregulated expression of S100A8 and S100A9 in adipose tissues of obese mice. *Biochem. Biophys. Res. Commun.* **419,** 782–789
68. Baumann, C. A., Ribon, V., Kanzaki, M., Thurmond, D. C., Mora, S., Shigematsu, S., Bickel, P. E., Pessin, J. E., and Saltiel, A. R. (2000) CAP defines a second signalling pathway required for insulin-stimulated glucose transport. *Nature* **407,** 202–207
69. Lin, W. H., Chiu, K. C., Chang, H. M., Lee, K. C., Tai, T. Y., and Chuang, L. M. (2001) Molecular scanning of the human sorbin and SH3-domain-containing-1 (SORBS1) gene: positive association of the T228A polymorphism with obesity and type 2 diabetes. *Hum. Mol. Genet.* **10,** 1753–1760
70. Zhang, D., Liu, Z. X., Choi, C. S., Tian, L., Kibbey, R., Dong, J., Cline, G. W., Wood, P. A., and Shulman, G. I. (2007) Mitochondrial dysfunction due to long-chain Acyl-CoA dehydrogenase deficiency causes hepatic steatosis and hepatic insulin resistance. *Proc. Natl. Acad. Sci. U.S.A.* **104,** 17075–17080
71. Deram, S., Nicolau, C. Y., Perez-Martinez, P., Guazzelli, I., Halpern, A., Wajchenberg, B. L., Ordovas, J. M., and Villares, S. M. (2008) Effects of perilipin (PLIN) gene variation on metabolic syndrome risk and weight loss in obese children and adolescents. *J. Clin. Endocrinol. Metab.* **93,** 4933–4940
72. Hwang, H., Bowen, B. P., Lefort, N., Flynn, C. R., De Filippis, E. A., Roberts, C., Smoke, C. C., Meyer, C., Hojlund, K., Yi, Z., and Mandarino, L. J. (2010) Proteomics analysis of human skeletal muscle reveals novel abnormalities in obesity and type 2 diabetes. *Diabetes* **59,** 33–42
73. Lu, H., Yang, Y., Allister, E. M., Wijesekara, N., and Wheeler, M. B. (2008) The identification of potential factors associated with the development of type 2 diabetes: a quantitative proteomics approach. *Mol. Cell. Proteomics* **7,** 1434–1451